JCTC Journal of Chemical Theory and Computation

Influence of Strong Electron Correlation on Magnetism in Transition-Metal Doped Si Nanocrystals

R. Leitsmann,[†] F. Küwen,[‡] C. Rödl, C. Panse, and F. Bechstedt*

European Theoretical Spectroscopy Facility (ETSF) and Institut für Festkörpertheorie und -optik, Friedrich-Schiller-Universität Jena, Max-Wien-Platz 1, 07743 Jena, Germany

Received July 31, 2009

Abstract: We studied the influence of strong electron correlation on magnetic properties of Si nanocrystals doped with the transition metal (TM) atoms Mn and Fe. Different approaches to describe exchange and correlation (XC) effects are compared within a density-functional framework. Beside a semilocal treatment, two different methods to include the influence of electron correlation on the localized TM 3d states are studied. They are based on XC functionals with the inclusion of on-site Coulomb repulsion or short-range screened exchange. We demonstrate a strong dependence of both electronic structure and magnetization on the used XC functional. The inclusion of strong correlation drastically changes position and occupation of the TM or TM−Si-bond-derived levels as well as the total magnetic moments.

Introduction

Nanostructuring of materials can lead to novel properties that do not exist in bulk-phase materials. In particular, nanocrystals (NCs) have a high potential for multimodal biological applications by the addition of functionality to augment their optical efficiency.[1−3] Due to the quantum confinement, NCs exhibit intense photoluminescence at wavelengths that can be tuned throughout the visible spectrum by changing the particle size.[4,5] Their biocompatibility, the high photoluminescence quantum efficiency, and the stability against photobleaching make silicon NCs ideal candidates for many biological imaging techniques.[6,7] The incorporation of magnetic 3d transition metal (TM) impurities in Si NCs would allow a combination of optical detection with magnetic resonance imaging techniques or magnetic separation. It has been shown experimentally and theoretically that doping of Si nanostructures with nonmagnetic impurities already leads to significantly modified properties with respect to the bulk Si case.[8−12]

The modification of the magnetic and electronic properties of Si nanostructures by TM atom doping is an exciting field. A central question concerns the influence of electron confinement on magnetism on a nanoscale, for example, the combination of possible ferromagnetism with a half-metallic character of the NC. Similar questions have been studied by means of spin-polarized density functional theory (DFT) for δ-doped layers of Mn in Si[13,14] and TM-doped Si nanowires.[15−17] Also, the spin polarization in Mn-doped Ge NCs and TM-doped Si NCs as well as its consequences have been investigated recently.[18−21] Self-organized $Ge_{1-x}Mn_x$ nanocolumns are found to tend to high-Curie-temperature ferromagnetism.[22]

However, there are serious limitations of such DFT[23] studies for localized electrons using local or semilocal approximations for exchange and correlation (XC) such as the local spin density approximation (LSDA) or the (spin-polarized) generalized gradient approximation (GGA). The electrons of the open 3d shell of TM atoms such as Mn and Fe are rather strongly localized. In transition metals and their oxides, for example, the 3d electrons experience strong Coulomb repulsion because of their spatial localization. Such strongly "interacting" or "correlated" electrons cannot be simply described as embedded in a mean field generated by the other electrons.[24] Frequently, this electron correlation is characterized by an empirical intra-atomic d−d Coulomb interaction U within DFT-based descriptions, so-called LDA+U or GGA+U methods,[25] or dynamical mean-field theory (DMFT).[24,26] Furthermore, for antiferromagnetic TM oxides, it has been demonstrated that effects related to the strong localization of the TM 3d states can be described by a spatially nonlocal potential derived from a hybrid XC functional which contains a screened exchange contribution.[27−30] Also, ferromagnetic systems may be modeled using such an approach.[31] The idea is, however, not to include simply the nonlocal Hartree−Fock exchange in which no correlation part is present. Rather, the use of a spatially nonlocal XC potential in the Kohn−Sham equation is considered as a zeroth-order approximation for the XC self-energy of the quasiparticle equation.[29,32] That allows the description of electronic single-quasiparticle excitations. Thereby, the screened Fock exchange

* Correponding author e-mail: bechsted@ifto.physik.uni-jena.de.

[†] Current address: GWT-TUD GmbH, Material Calculations, Annabergerstr. 240, 09125 Chemnitz, Germany.

[‡] Current address: Energieforschungszentrum Niedersachsen, Technische Universität Clausthal, Am Stollen 19, 38640 Goslar, Germany.

10.1021/ct9003993 © 2010 American Chemical Society
Published on Web 01/22/2010

with a modified Coulomb potential and a prefactor α, whose reciprocal value can be identified with a static background dielectric constant, is used. In any case, screened exchange as the most important effect for the widening of the energetic distances between occupied and empty single-electron states is taken into account.

Theoretical Description

The influence of strong electron correlation effects of d electrons in nanoscale systems and its interplay with the spatial confinement of s and p electrons are barely investigated so far. For that reason, we study the electronic and magnetic properties of TM-doped Si NCs in the framework of three different approaches to XC in this work: semilocal GGA,[33] the inclusion of an additional Coulomb repulsion U within GGA+U,[34] as well as a description of XC using the hybrid functional HSE03,[35,36] which accounts for nonlocal screened exchange. Within the GGA+U scheme of Dudarev et al.,[34] which is applied here, only an effective parameter U representing the difference between the on-site Coulomb repulsion and the exchange parameter is meaningful. For both Mn 3d and Fe 3d electron systems, we use an effective $U = 3$ eV that is somewhat smaller than that from earlier suggestions.[25] With the study of quasiparticle band structures of TM monoxides,[30] however, it has been found that larger values of U give rise to wrong band orderings. Test calculations showed that an increase of U up to 5 eV does not change the electronic properties of the NCs qualitatively.

The atomic positions of the atoms in the Si NCs are determined by a shell-by-shell construction procedure which starts from a central atom and successively adds shells of Si atoms.[37] This results in faceted Si NCs with six {100} and eight {111} facets whose surface dangling bonds are passivated by H atoms. Periodic arrangements of simple cubic supercells with sufficiently large edge lengths guarantee a distance larger than 1 nm between the surfaces of NCs in adjacent supercells. The atomic geometry of the clean and doped NCs is optimized using a DFT-GGA framework as implemented in the Vienna ab initio simulation package.[38] Pseudopotentials are generated within the projector-augmented wave method,[39] which allows for an accurate description of the (all-electron) wave functions in the core region. An energy cutoff of 200 eV is used for the plane-wave expansion.

Results and Discussion

The energetic stability of the dopant arrangement has been studied in the framework of DFT-GGA and GGA+U for both Mn and Fe atoms for different substitutional doping positions, as indicated in Figure 1. The results yield a tendency of the TM atoms to occupy either the NC center or subsurface positions.[40] In the light of these results, we focus our attention on substitutional sites in the center position of the NC to retain an atomic geometry with T_d point-group symmetry. Interstitial sites and arbitrary sites outside the NC center would give rise to a lowering of the point-group symmetry and, hence, a splitting of the defect levels. Such splittings hamper a clear identification of the effects resulting from different treatments of XC.[21] Therefore, the T_d symmetry of the NCs is enforced during the minimization of the total energy with respect to the structural

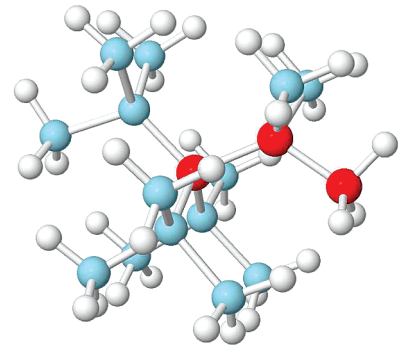

Figure 1. Stick-and-ball model of a $Si_{17}H_{36}$ nanocrystal with Si atoms (cyan/light gray) and H atoms (white). The three possible substitutional positions for TM atoms are indicated as red/dark gray balls.

degrees of freedom. In the case of the variation of the electronic degrees of freedom, we lift the symmetry constraint in order to allow for arbitrary level occupancies and accompanying level splittings. Nevertheless, the impurity levels, especially those derived from TM 3d states, will be still classified by e and t_2 states. This procedure allows us a more precise discussion of the effects of the electron−electron interaction beyond the semilocal XC approach. Our GGA studies (not presented here) show a relatively weak dependence of the qualitative and absolute arrangement of the impurity levels with respect to energetic position and spin channel on the NC size. The main effect concerns the gap size, as for undoped Si NCs. On the other hand, numerical calculations within the hybrid XC functional framework are prohibitive for large NCs for computer-time reasons. Therefore, we restrict the studies to the model system of $Si_{16}H_{36}TM$ (TM = Mn, Fe) nanocrystals where the central Si atom is replaced by a TM atom.

The energy levels obtained for the NCs within the three different XC treatments GGA, GGA+U, and HSE03 are presented in Figures 2 (Mn doping) and 3 (Fe doping). The states with e and t_2 symmetry and their occupation are indicated for both the majority and minority spin channels. Because of the interaction with the surrounding Si atoms, t_2 states with bonding and antibonding character appear. One observes a significant influence of the description of exchange and correlation using a hybrid functional (HSE03) or adding an on-site Coulomb repulsion (GGA+U) in comparison to the pure semilocal approximation (GGA).

Within the GGA approach, the TM 3d-derived impurity states appear in the vicinity of the fundamental gap of the undoped NC. These impurity levels, which are described and classified in terms of nonbonding states with e character and t_2 bonding and antibonding states between TM 3d and Si $3sp^3$ orbitals, and their occupation can be explained within a defect molecule model.[41] Nine (ten) electrons are available to occupy these Mn(Fe)-derived defect levels in the two spin channels. For both spin channels, the t_2 levels with strong bonding (antibonding) character are fully occupied (remain empty). Consequently, the chemical bonding causes a violation of Hund's rule, which is valid for the free TM atoms. The almost half-metallic (Mn) or insulating (Fe) character of the TM-doped Si NCs is related to the occupation of the nonbonding e levels. For doping with Fe, that is, a dopant with an even number of 3d electrons, the e

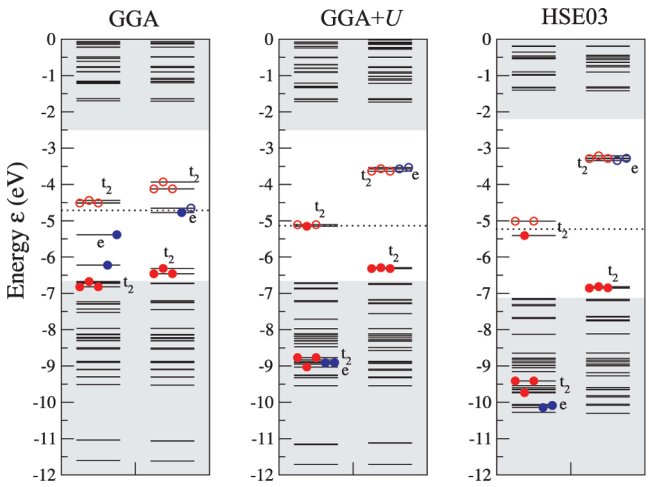

Figure 2. Energy level schemes for a $Si_{16}H_{36}Mn$ nanocrystal with a central Mn atom obtained within (a) GGA, (b) GGA+*U*, and (c) HSE03 for the majority spin channel (left) and minority spin channel (right). The vacuum level is used as common energy zero. The Fermi level is given as a dotted horizontal line. The fundamental gap region of the undoped $Si_{17}H_{36}$ crystal is indicated by a white background. The occupation of levels with *e* (blue) and t_2 (red) symmetry is denoted by filled red circles or empty circles, respectively.

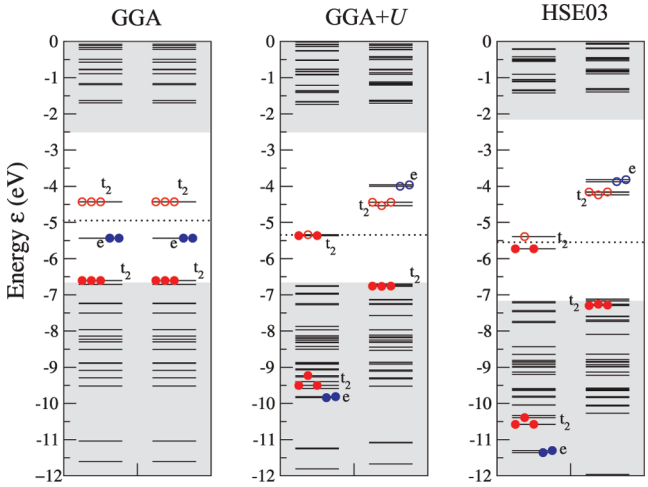

Figure 3. As in Figure 2 but with Fe instead Mn.

levels in both spin channels are completely filled. The doped Si NC appears to be spin-unpolarized, that is, possesses a vanishing magnetic moment. In the Si NC doped with Mn featuring five 3d electrons, one *e* level remains empty. Taking into account the very small gap between the two *e* levels, this results in an almost half-metallic system with low spin polarization and a magnetic moment of about 1 μ_B. In summary, low-spin configurations with $S = 1/2$ (Mn) or $S = 0$ (Fe) appear. The findings for the magnetic moments are almost in agreement with earlier GGA predictions.[20]

The inclusion of XC effects beyond GGA within the HSE03 functional or the GGA+*U* approach yields a completely different electronic structure of the doped Si NCs in Figure 2 and Figure 3, since the positions and occupation of the impurity-derived levels are altered. Thereby, the differences due to the different XC treatment within the HSE03 and GGA+*U* approaches are small. The main effect is already visible within the GGA+*U* approach: Fully occupied (empty) levels with strong TM 3d character are shifted toward lower (higher) energies, while impurity states mainly localized at the four Si neighbors remain less influenced. In the majority and minority spin channels, splittings of the t_2-derived levels with their occupation appear for all studied treatments of XC. However, these splittings are much larger within the HSE03 approach, which is the result of the spin dependence of the Fock part in the HSE03 functional. Exchange only acts on parallel spins and mostly influences the occupied states by lowering them in energy. As a consequence, the occupied t_2 and *e* levels with mainly TM 3d character shift toward lower energies and the empty levels in the opposite direction, similar to that within the GGA+*U* scheme. Thus, the nonbonding *e* states of the minority spin channel become unoccupied, and one additional electron occurs in the majority spin channel, resulting in spin-polarized NCs. A simple count of the difference of the electron numbers in the spin channels gives magnetic moments of 3 μ_B (Mn) or 4 μ_B (Fe). Consequently, the XC treatments beyond the semilocal GGA stabilize high-spin configurations with $S = 3/2$ (Mn) or $S = 2$ (Fe).

The Fermi level positions and the magnetic moments of the NCs depend strongly on their electronic structure and, hence, on the strong electron correlation effects. The account for on-site electron−electron interaction between the localized TM 3d electrons within the GGA+*U* and HSE03 frameworks influences the absolute energetic positions of the occupied and empty mainly 3d-derived states with *e* and t_2 symmetry. On the other hand, the t_2 levels in the minority spin channel with strong Si sp^3 character remain almost uninfluenced. Consequently, a complete change of the gap states occurs going beyond the (semi)local approximation for XC. A level mainly related to Si-derived t_2 defect states appears in a midgap position of the majority spin channel. The 3-fold degeneracy of this level is lifted due to an electronic Jahn−Teller effect. The lifted degeneracy of the Si-related t_2 defect level does not influence the high-spin state of the doped NC and the accompanying magnetic moment $\mu = 3\ \mu_B$ (Mn) or 4 μ_B (Fe). However, in contrast to the almost half-metallic character within the GGA (Mn) and GGA+*U* (Mn, Fe) approaches, the NC becomes insulating within the HSE03 treatment for both types of TM atoms, Mn and Fe.

Since the ground state is given by a single Slater determinant in DFT, problems concerning the description of spin multiplets arise.[43] It is also difficult to find the global minimum of the total energy with respect to the spin polarization. We have, therefore, carefully studied the total energy of the NC versus the local magnetic moment μ of the TM ions. We start the self-consistent procedure with large magnetic moments of the TM atoms (being typically by 2 μ_B larger than the "expected" value). During the electronic relaxation, the value of the magnetization is significantly reduced. Whereas within GGA only a global minimum for the low-spin configuration with $\mu = 1$ (0) μ_B was found for TM = Mn (Fe), several local minima occur for the GGA+U and HSE03 treatments, whereas the global one corresponds to the high-spin state. For TM = Mn, we compute an energy gain of 0.63 (0.65) eV for $\mu = 3\ \mu_B$ compared to $\mu = 1\ \mu_B$ within the GGA+*U* (HSE03) framework. In the TM =

Fe case, the situation is more complex. The high-spin state $\mu = 4\ \mu_B$ is lower in energy by 0.14 (0.06) eV or 0.34 (−0.04) eV with respect to the intermediate-spin state $\mu = 2\ \mu_B$ or low-spin state $\mu = 0\ \mu_B$ using the GGA+U (HSE03) method. That means that the total energy only weakly varies as a function of the local magnetization using the hybrid functional.

The question arises whether the obtained results follow a defect-molecule model with a central TM dopant and four nearest-neighbor Si atoms characterized by strong chemical bonding or whether such a picture is destroyed due to the strong correlation effects. To clarify this question, we neglect electronic confinement effects and compare with results for a substitutional TM doping in bulk Si, here, simulated by one TM atom in a simple cubic (sc) unit cell containing 216 atoms. For the Brillouin zone sampling, a 5 × 5 × 5 Monkhorst-Pack mesh is used. Thereby, we restrict ourselves to the GGA and GGA+U treatments. The corresponding densities of states (DOS) are presented in Figure 4 for both spin channels. Because of computer-time limitations, we perform the hybrid-functional computations only for the Γ point. This allows us at least to compare the relative level position in the bulk case with those for the Si NCs. Also in the bulk limit, the inclusion of the on-site interaction changes the defect-induced levels in the fundamental gap region dramatically. The half-metallic character is conserved for Mn in Si, whereas for Fe in Si the on-site interaction U destroys the insulating character and also gives rise to a half metal with partially occupied states in the majority spin channel. The results for the energy levels and their occupation are very similar to those observed in Figures 2 and 3 for the TM-doped $Si_{17}H_{36}$ nanocrystals. This holds for the relative level position and the level occupation; only the fundamental gap is much smaller. Qualitatively, the same holds for an HSE03 treatment. We conclude that the electron confinement effects influence the energy scale but not the qualitative impurity level arrangement. Such similarities of the TM impurity behavior in Si NCs and bulk Si are also observed for the magnetic moments with $\mu = 1.0$ (GGA, Mn), ∼ 0 (GGA, Fe), 3.0 (GGA+U, Mn), 4.0 (GGA+U, Fe), 3.0 (GGA+HSE03, Mn), and 4.0 μ_B (GGA+HSE03, Fe). The reason for this congenerous behavior is closely related to the strong localization of the TM 3d states at the impurity sites: These states are hardly influenced by additional confinement effects due to the finite size of the NCs. Therefore, in Si NCs, the impurity levels exhibit a similar magnetic character as isolated TM impurities in bulk Si.

The comparison of these results with other theoretical investigations is somewhat puzzling, because of different numerical and methods and treatments of XC. For example, for bulk Si, the Green's function approach of Beeler et al.[42] predicts magnetic moments of 3 (Mn) and 0 μ_B (Fe), which agree completely neither with the GGA nor with the GGA+U results. Only in the limit of higher TM concentrations, for example, described by one TM atom in a 32-atom supercell, GGA also yields $\mu = 3$ (Mn) and 0 μ_B (Fe). On the other hand, the GGA+U results for bulk Si are fully consistent with the empirical rules of the Ludwig-Woodbury model, which predicts a total electron spin $S = N_e/2$, where N_e is the number of electrons occupying the antibonding t_2 and nonbonding e states (3 for Mn and 4 for Fe).[44] Strong electron correlation seems to be very important to fulfill the empirical rules for all situations. Due to the observed similarities of TM doping on the nanoscale and in bulk Si, the Ludwig-Woodbury model appears to be also applicable for nanostructures.

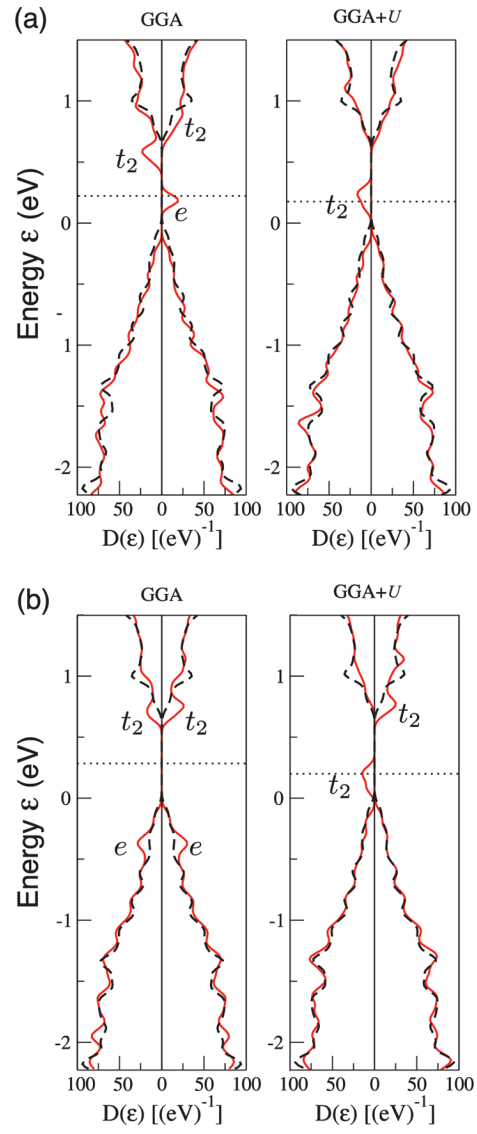

Figure 4. Densities of state $D(\varepsilon)$ of bulk Si doped with (a) Mn and (b) Fe at a substitutional position (red solid line) for the majority (left panel) and minority (right panel) spin channels. The bulk Si DOS (black dashed line) is shown for comparison. All DOSs are broadened using gaussians with the broadening parameter 0.1 eV. The horizontal dotted line indicates the Fermi level. The top of the valence bands of bulk Si is taken as energy zero. The main orbital character of the TM 3d-derived states close to the fundamental band gap is indicated.

Summary

We have studied the influence of strong electron correlation effects on the electronic and magnetic properties of transition-metal doped Si NCs for highly symmetric atomic geometries. The results clearly indicate that the properties of the NCs, especially those related to the 3d shell of the dopants, depend strongly on the treatment of exchange and correlation. Thus, electron correlation due to the strong localization of the 3d

electrons has to be taken into account beyond a (semi)local XC approximation. The GGA+U approach gives rise to a completely changed level ordering in the fundamental gap region compared to a GGA treatment. A refined approach to exchange and correlation taking into account occupation-induced splittings within the HSE03 hybrid functional yields the same magnetic properties as GGA+U. Since the results are similar to the situation of TM doping of bulk silicon, the electron confinement seems not to enhance the effects of electron correlation and magnetic properties, and the magnetization still follows the Ludwig-Woodbury rules.

Acknowledgment. We gratefully acknowledge discussions with J. Furthmüller. Financial support was provided by the FWF Austria via SFB25 IR-ON, the Deutsche Forschungsgemeinschaft (Project No. Be1346/20-1), and the European Community within e-I3 project ETSF (GA No. 211956). We thank the Leibniz Rechenzentrum München and the HLRS in Stuttgart for grants of computer time.

References

(1) Huh, Y.-M.; Jun, Y.-w.; Song, H.-T.; Kim, S; Choi, J.-s.; Lee, J.-H.; Yoon, S.; Kim, K.-S.; Shin, J.-S.; Suh, J.-S.; Cheon, J. In Vivo Magnetic Resonance Detection of Cancer by Using Multifunctional Magnetic Nanocrystals. *J. Am. Chem. Soc.* **2005**, *127*, 12387.

(2) Santra, S.; Yang, H.; Holloway, P. H.; Stanley, J. T.; Mericle, R. A. Synthesis of Water-Dispersible Fluorescent, Radio-Opaque, and Paramagnetic CdS:Mn/ZnS Quantum Dots: A Multifunctional Probe for Bioimaging. *J. Am. Chem. Soc.* **2005**, *127*, 1656.

(3) Michalet, X; Pinaud, F. F.; Bentolila, L. A.; Tsay, J. M.; Doose, S; Li, J. J.; Sundaresan, G; Wu, A. M.; Gambhir, S. S.; Weiss, S. Quantum Dots for Live Cells, in Vivo Imaging, and Diagnostics. *Science* **2005**, *307*, 538.

(4) Canham, L. T. Silicon quantum wire array fabrication by electrochemical and chemical dissolution of wafers. *Appl. Phys. Lett.* **1990**, *57*, 1046.

(5) Veinot, J. G. C. Synthesis, surface functionalization, and properties of freestanding silicon nanocrystals. *Chem. Commun.* **2006**, 4160.

(6) Li, Z. F.; Ruckenstein, E. Water-Soluble Poly(acrylic acid) Grafted Luminescent Silicon Nanoparticles and Their Use as Fluorescent Biological Staining Labels. *Nano Lett.* **2004**, *4*, 1463.

(7) Wang, L; Reipa, V; Blasic, J. Silicon Nanoparticles as a Luminescent Label to DNA. *Bioconjugate Chem.* **2004**, *15*, 409.

(8) Melnikov, D. V.; Chelikowsky, J. R. Quantum Confinement in Phosphorus-Doped Silicon Nanocrystals. *Phys. Rev. Lett.* **2004**, *92*, 046802.

(9) Ossicini, S.; Degoli, E.; Iori, F.; Luppi, E.; Magri, R.; Cantelle, G.; Trani, F.; Ninno, D. Simultaneously B- and P-doped silicon nanoclusters: Formation energies and electronic properties. *App. Phys. Lett.* **2005**, *87*, 173120.

(10) Fujii, M.; Yamaguchi, Y.; Takase, Y.; Ninomiya, K.; Hayashi, S. Photoluminescence from impurity codoped and compensated Si nanocrystals. *Appl. Phys. Lett.* **2005**, *87*, 211919.

(11) Pi, X. D.; Gresback, R.; Liptak, R. W.; Campell, S. A.; Kortshagen, U. Doping efficiency, dopant location, and oxidation of Si nanocrystals. *Appl. Phys. Lett.* **2008**, *92*, 123102.

(12) Xu, Q.; Luo, J.-W.; Li, S.-S.; Xia, J.-B.; Li, J.; Wei, S.-H. Chemical trends of defect formation in Si quantum dots: The case of group-III and group-V dopants. *Phys. Rev. B* **2007**, *75*, 235304.

(13) Qian, M. C.; Fong, C. Y.; Liu, K.; Pickett, W. E.; Pask, J. E.; Yang, L. H. Half-Metallic Digital Ferromagnetic Heterostructure Composed of a δ-Doped Layer of Mn in Si. *Phys. Rev. Lett.* **2006**, *96*, 027211.

(14) Wu, H.; Kratzer, P.; Scheffler, M. Density-Functional Theory Study of Half-Metallic Heterostructures: Interstitial Mn in Si. *Phys. Rev. Lett.* **2007**, *98*, 117202.

(15) Durgun, E.; Cakir, D.; Akman, N.; Ciraci, S. Half-Metallic Silicon Nanowires: First-Principles Calculations. *Phys. Rev. Lett.* **2007**, *99*, 256806.

(16) Durgun, E.; Akman, N.; Ciraci, S. Functionalization of silicon nanowires with transition metal atoms. *Phys. Rev. B* **2008**, *78*, 195116.

(17) Xu, Q.; Li, J.; Li, S.-S.; Xia, J.-B. The formation and electronic structures of 3d transition-metal atoms doped in silicon nanowires. *J. Appl. Phys.* **2008**, *104*, 084307.

(18) Huang, X.; Makmal, A.; Chelikowsky, J. R.; Kronik, L. Size-Dependent Spintronic Properties of Dilute Magnetic Semiconductor Nanocrystals. *Phys. Rev. Lett.* **2005**, *94*, 236801.

(19) Arantes, J. T.; Dalpian, G. M.; Fazzio, A. Quantum confinement effects on Mn-doped InAs nanocrystals: A first-principles study. *Phys. Rev. B* **2008**, *78*, 045402.

(20) Ma, L. T.; Zhao, J.; Wang, J.; Wang, B.; Wang, G. Magnetic properties of transition-metal impurities in silicon quantum dots. *Phys. Rev. B* **2007**, *75*, 045312.

(21) Leitsmann, R.; Panse, C.; Küwen, F.; Bechstedt, F. Ab initio characterization of transition-metal-doped Si nanocrystals. *Phys. Rev. B* **2009**, *80*, 104412.

(22) Jamet, M.; Barski, A.; Devillers, T.; Poydenot, V.; Dujardin, R.; Bayle-Guillemaud, P.; Rothman, J.; Bellet-Amalric, E.; Marty, A.; Cibert, J.; Mattana, R.; Tatarenko, S. High-Curie-temperature ferromagnetism in self-organized Ge 1_x Mn_x nanocolumns. *Nature Mat.* **2006**, *5*, 653.

(23) Kohn, W.; Sham, L. J. Self-Consistent Equations Including Exchange and Correlation Effects. *Phys. Rev.* **1965**, *140*, A1133.

(24) Imada, M.; Fujimori, A.; Tokura, Y. Metal-insulator transitions. *Rev. Mod. Phys.* **1998**, *70*, 1039.

(25) Anisimov, V. I.; Zaanen, J.; Andersen, O. K. Band theory and Mott insulators: Hubbard U instead of Stoner I. *Phys. Rev. B* **1991**, *44*, 943.

(26) Biermann, S.; Aryasetiawan, F.; Georges, A. First-Principles Approach to the Electronic Structure of Strongly Correlated Systems: Combining the GW Approximation and Dynamical Mean-Field Theory. *Phys. Rev. Lett.* **2003**, *90*, 086402.

(27) Franchini, C.; Bayer, V.; Podloucky, R.; Paier, J.; Kresse, G. Density functional theory study of MnO by a hybrid functional approach. *Phys. Rev. B* **2005**, *72*, 045132.

(28) Marsman, M.; Paier, J.; Stroppa, A.; Kresse, G. Hybrid functionals applied to extended systems. *J. Phys.: Condens. Matter* **2008**, *20*, 064201.

(29) Rödl, C.; Fuchs, F.; Furthmüller, J.; Bechstedt, F. Ab initio theory of excitons and optical properties for spin-polarized systems: Application to antiferromagnetic MnO. *Phys. Rev. B* **2008**, *77*, 184408.

(30) Rödl, C.; Fuchs, F.; Furthmüller, J.; Bechstedt, F. Quasiparticle band structures of the antiferromagnetic transition-metal oxides MnO, FeO, CoO, and NiO. *Phys. Rev. B* **2009**, *79*, 235114.

(31) Wilson, N. C.; Russo, S. P. Hybrid density functional theory study of the high-pressure polymorphs of α-Fe_2O_3 hematite. *Phys. Rev. B* **2009**, *79*, 094113.

(32) Fuchs, F.; Furthmüller, J.; Bechstedt, F.; Shishkin, M.; Kresse, G. Quasiparticle band structure based on a generalized Kohn-Sham scheme. *Phys. Rev. B* **2007**, *76*, 115109.

(33) Perdew, J. P.; Wang, Y. Accurate and simple analytic representation of the electron-gas correlation energy. *Phys. Rev. B* **1992**, *45*, 13244.

(34) Dudarev, S. L.; Botton, G. A.; Savrasov, S. Y.; Humphreys, C. J.; Sutton, A. P. Electron-energy-loss spectra and the structural stability of nickel oxide: An LSDA+U study. *Phys. Rev. B* **1998**, *57*, 1505.

(35) Heyd, J.; Scuseria, G. E.; Ernzerhof, M. Hybrid functionals based on a screened Coulomb potential. *J. Chem. Phys.* **2003**, *118*, 8207.

(36) Krukau, A.; Vydrov, O.; Izmaylov, A.; Scuseria, G. Influence of the exchange screening parameter on the performance of screened hybrid functionals. *J. Chem. Phys.* **2006**, *125*, 224106.

(37) Ramos, L. E.; Furthmüller, J.; Bechstedt, F. Effect of backbond oxidation on silicon nanocrystallites. *Phys. Rev. B* **2005**, *70*, 033311.

(38) Kresse, G.; Furthmüller, J. Efficiency of ab-initio total energy calculations for metals and semiconductors using a plane-wave basis set. *Comput. Mater. Sci.* **1996**, *6*, 15.

(39) Kresse, G.; Joubert, D. From ultrasoft pseudopotentials to the projector augmented-wave method. *Phys. Rev. B* **1999**, *59*, 1758.

(40) Küwen, F.; Leitsmann, R.; Bechstedt, F. Mn and Fe doping of bulk Si: Concentration influence on electronic and magnetic properties. *Phys. Rev. B* **2009**, *80*, 45203.

(41) Enderlein, R.; Horing, N. In *Fundamentals of Semiconductor Physics and Devices*; World Scientific: London, 1997; p 285.

(42) Beeler, F.; Andersen, O.; Scheffler, M. Electronic and magnetic structure of 3d transition-metal point defects in silicon calculated from first principles. *Phys. Rev. B* **1990**, *41*, 1603.

(43) Zywietz, A.; Furthmüller, J.; Bechstedt, F. Spin state of vacancies: From magnetic Jahn-Teller distortions to multiplets. *Phys. Rev. B* **2000**, *62*, 6854.

(44) Ludwig, G.; Woodbury, H. In *Solid State Physics*; Academic: New York 1962; Vol. 13, p 331.

CT9003993